Inorg. Chem. **2003**, *42*, 7852–7860

Time-Dependent Density Functional Theory Study of the Spectroscopic Properties Related to Aggregation in the Platinum(II) Biphenyl Dicarbonyl Complex

Stanislav R. Stoyanov, John M. Villegas, and D. Paul Rillema*

Department of Chemistry, Wichita State University, Wichita, Kansas 67260-0051

Received March 3, 2003

Singlet ground-state geometry optimization of the monomer, four dimers, and the trimer of $[Pt(bph)(CO)_2]$, where bph = biphenyl dianion, was performed at the B3LYP level of density functional theory (DFT) with a mixed basis set (6-311G** on C, O, and H atoms; the Stuttgart/Dresden (SDD) effective core potential (ECP) on the Pt core; [6s5p3d] on the Pt valence shell). The aggregation was based on Pt–Pt binding as well as on π–π and electrostatic interactions. The lowest-lying triplet-state geometries of the monomer, one dimer, and the trimer of the complex were also optimized using the above theory. Significant shortening of the Pt–Pt bond was recorded in the triplet state compared to the singlet one. A number of low-energy singlet and triplet allowed excited states were calculated using time-dependent density functional theory (TDDFT) and analyzed with respect to absorption, excitation, and emission spectra collected under various conditions. Simulated spectra of the monomer and dimer based on the singlet excited states were correlated with the absorption spectrum. The emission in concentrated solution was due to the triplet dimer, and the emitting states were ^{3}MLCT and Pt-centered states.

Introduction

Square planar polypyridyl and biphenyl complexes of Pt(II) are known to crystallize in linear chains resulting in metal−metal interactions. The emission properties of such crystals have been extensively investigated,[1−4] and it is found that the binding modes can alter the emission significantly. Neutral complexes, such as $[Pt(bpy)(CN)_2]$ (bpy = 2,2′-bipyridine), form linear chains of equidistant complexes, stacked along the Pt−Pt bond.[1] Cationic complexes, like $[Pt(phbpy)Cl]^+$ (phbpy = 6-phenyl-2,2′-bipyridine), crystallize in dimers (alternating short and long Pt−Pt distances along the chain).[2] Dianions, like $[Pt(CN)_4]^{2-}$, form both equidistant and alternating linear chains, depending on the counterion.[3] Double salts, like $[Pt(bpy)_2][Pt(CN)_4]$, form linear chain polymers, and their electronic spectra are strongly perturbed from those of the monomers.[4] One-electron band structure model calculations for a linear chain of $[Pt(CN)_4]^{2-}$ were used to explain the dominance of the Pt $5d_{z^2}$ and Pt $6p_z$ orbitals responsible for the red shift of the main optical transitions with decreasing Pt−Pt distance.[5] However, it is experimentally found that the emission behavior of these complexes is determined by states that are localized in clusters of a few complexes only.[3]

In dilute solution it is thought that the neutral complexes exist as monomers. There are reports, however, that suggest a concentration and solvent dependence of the spectral behavior. It was proposed that aggregation starts at certain limiting concentrations, depending on the donor number of the solvent.[6,7] The two possible interactions that would determine the type of aggregate were metal−metal interaction and π−π stacking.[1,8,9]

Density functional theory (DFT)-calculated molecular orbital distributions have been very useful for the interpreta-

* Author to whom correspondence should be addressed. E-mail: paul.rillema@wichita.edu.

(1) Connick, W. B.; Marsh, R. E.; Schaefer, W. P.; Gray, H. B. *Inorg. Chem.* **1997**, *36*, 912−922.
(2) Ratilla, E. M. A.; Scott, B. K.; Moxness, M. S.; Kostic, N. M. *Inorg. Chem.* **1990**, *20*, 918−926.
(3) Gliemann, G.; Yersin, H. *Struct. Bonding (Berlin)* **1985**, *62*, 87−161.
(4) Miskowski, V. M.; Houlding, V. H. *Inorg. Chem.* **1991**, *30*, 4446−4452.
(5) Interrante, L. V.; Messmer, R. P. In *Extended Interactions between Metal Ions in Transition Metal Complexes*; Interrante, L. V., Ed.; ACS Symposium Series 5; American Chemical Society: Washington, DC, 1974; p 382.
(6) Zheng, G. Y.; Rillema, D. P. *Inorg. Chem.* **1998**, *37*, 1392−1397.
(7) Ardasheva, L. P.; Shagisultanova, G. A. *Zh. Neorg. Khim.* **1998**, *43*, 92−99.
(8) Fleeman, W. L.; Connick, W. B. *Spectrum (Bowling Green, OH, US)* **2002**, *15*, 14−19.
(9) Chan, C. W.; Lai, T. F.; Che, C. M.; Peng, S. M. *J. Am Chem. Soc.* **1993**, *115*, 11245−11253.

10.1021/ic030084n CCC: $25.00
Published on Web 10/31/2003

tion of electrochemical and photochemical results for Ru(II) complexes.[10] The frontier orbital spatial distributions calculated using the B3LYP/3-21G(*) method were found to track well the observed site of the electrochemical reductions for a ferrocene−C_{60}−dinitrobenzene triad.[11] A DFT study of the energetics and the reaction path in a series of S_N2 reactions of square planar Pt(II) complexes with H_2O, NH_3, and chloride ligands ruled out the presence of an intermediate but supported the existence of a single transition state.[12]

Time-dependent density functional theory (TDDFT) has recently become a reliable method for calculation of excited-state energies and has proven useful in the assignment of the electronic singlet excited states to the absorption spectra of systems as complex as Ru(II) and Cr(III) polypyridyl complexes.[13−15] Molar absorptivities were calculated based on the values of oscillator strengths for the excited states and were found to be in close agreement with experimental ones.[13] Triplet excited states calculated using TDDFT were applied to the interpretation of the emission behavior of complexes of W(0) with CO and diimine ligands.[16] Calculated singlet−triplet splittings and vertical triplet−triplet excitation energies for a series of π-conjugated organic and organometallic chromophores were found to be in good agreement with the experimental spectra.[17]

We initiated an investigation of the excited-state properties of [Pt(bph)$(CO)_2$] in an attempt to elucidate the aggregation processes in concentrated solutions and to clarify the identity of the "oligomers" responsible for the triplet excited-state properties of single crystals and species present in concentrated solutions.

Calculations and Results

The geometries and the electronic structures of the monomer, several dimers, and the trimer of [Pt(bph)$(CO)_2$] were optimized in the singlet ground state using Becke's three-parameter hybrid functional B3LYP[18] with the local term of Lee, Yang, and Parr[19] and the nonlocal term of Vosko, Wilk, and Nassiar[20] and with the Gaussian 98 (ver 5.4, rev A.9) program package. The Stuttgart/Dresden (SDD) effective core potential (ECP)[21] was used for the Pt core potential and the (8s7p6d)/[6s5p3d] Gaussian-type orbital (GTO) was used for the valence shell together with the all-electron 6-311G** basis set[22,23] for the C, O, and H atoms of [Pt(bph)$(CO)_2$]. The lowest-lying triplet-state geometries of the monomer, dimer **A**, and the trimer (Figure 1) were also determined using the same theory.

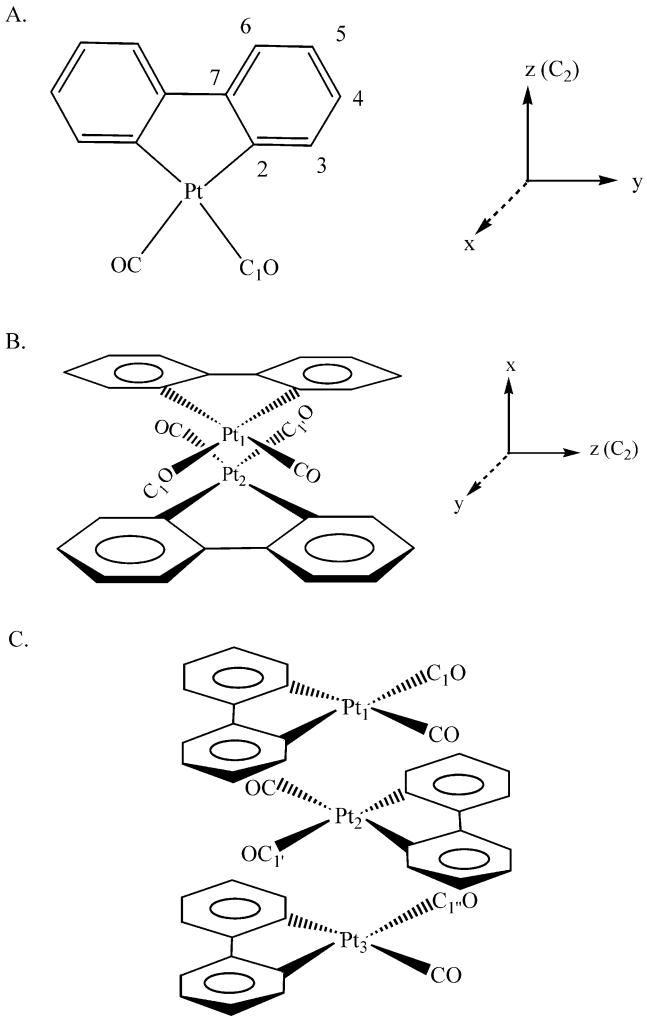

Figure 1. Coordinate systems and rotation axes for [Pt(bph)$(CO)_2$]: (A) monomer (C_{2v}); (B) dimer **A** (C_{2h}); (C) trimer (C_s).

The geometry of the monomer was optimized in C_{2v} symmetry (Figure 1A) as determined from X-ray diffraction.[24] Dimer **A** (Figure 1B and Table 1) was optimized in C_{2h} symmetry, whereas the trimer was optimized in C_s symmetry (Figure 1C), where the plane of symmetry was defined by the three Pt atoms. Two monomer units were used for the geometry optimization of the dimers, and the input structures were prepared as described below. For the torsion angle C1−Pt1−Pt2−C1′ the initial value of 180° was used for dimers **A** and **D**. The initial value of 0° was used for dimers **B** and **C** (Figures 1B and 2). The above torsion angles were subjected to geometry optimization to yield 180.0° for dimer **A**, 0.2° for dimer **B**, 6.5° for dimer **C**, and 175.9° for

(10) Villegas, J. M.; Stoyanov, S. R.; Rillema, D. P. *Inorg. Chem.* **2002**, *41*, 6688−6694.
(11) D'Souza, F.; Zandler, M. E.; Smith, P. M.; Deviprasad, G. R.; Klykov, A.; Fujitsuka, M.; Ito, O. *J. Phys. Chem. A* **2002**, *106*, 649−656.
(12) Cooper, J.; Ziegler, T. *Inorg. Chem.* **2002**, *41*, 6614−6622.
(13) Monat, J. E.; Rodriguez, J. H.; McCusker, J. K. *J. Phys. Chem. A* **2002**, *106*, 7399−7406.
(14) Rodrigues, J. H.; Wheeler, D. E.; McCusker, J. K. *J. Am. Chem. Soc.* **1998**, *120*, 12051−12068.
(15) Zheng, K.; Wang, J.; Peng, W.; Liu, X.; Yun, F. *J. Phys. Chem. A* **2001**, *105*, 10899−10905.
(16) Farrell, I. R.; van Slageren, J.; Zalis, S.; Vlcek, A. *Inorg. Chim. Acta* **2001**, *315*, 44−52.
(17) Nguyen, K. A.; Kennel, J.; Pachter, R. *J. Chem. Phys.* **2002**, *117*, 7128−7136.
(18) Becke, A. D. *J. Chem. Phys.* **1993**, *98*, 5648−5652.
(19) Lee, C.; Yang, W.; Parr, R. G. *Phys. Rev. B: Condens. Matter Mater. Phys.* **1988**, *37*, 785−789.
(20) Vosko, S. H.; Wilk, L.; Nusair, M. *Can. J. Phys.* **1980**, *58*, 1200−1211.
(21) Andrae, D.; Hauessermann, U.; Dolg, M.; Stoll, H.; Preuss, H. *Theor. Chim. Acta* **1990**, *77*, 123−141.
(22) McLean, A. D.; Chandler, G. S. *J. Chem. Phys.* **1980**, *72*, 5639.
(23) Krishnan, R.; Binkley, J. S.; Seeger, R.; Pople, J. A. *J. Chem. Phys.* **1980**, *72*, 650.
(24) Chen, Y.; Merkert, J. W.; Murtaza, Z.; Woods, C.; Rillema, D. P. *Inorg. Chim. Acta* **1995**, *240*, 41−47.

Table 1. Selected Geometry Parameters of [Pt(bph)(CO)$_2$] Taken from X-ray Crystallography (ref 24) and Calculated Singlet Ground-State and Lowest-Lying Triplet-State Geometries Using B3LYP Theory and the 6-311G** Basis Set on the C, O, and H Atoms and the SDD ECP on the Pt Atom[a]

source	Pt−Pt, Å	Pt1−Pt2−Pt3, deg	Pt−C2, Å	Pt−C1, Å	C1−O, Å	C7−C7′, Å	C1−Pt−C1′, deg	C2−Pt−C2′, deg
X-ray	3.2426(3)	162.1	2.04(2)	1.98(2)	1.10(2)	1.40(3)	94.5(10)	80.5(8)
singlet	3.48	166.1	2.07	1.98	1.13	1.47	95.1	80.1
triplet	3.34	176.8	2.06	1.97	1.14	1.44	94.0	80.1

[a] The calculated results are for the monomer except for the Pt−Pt distance (dimer **A**) and Pt1−Pt2−Pt3 angle (trimer).

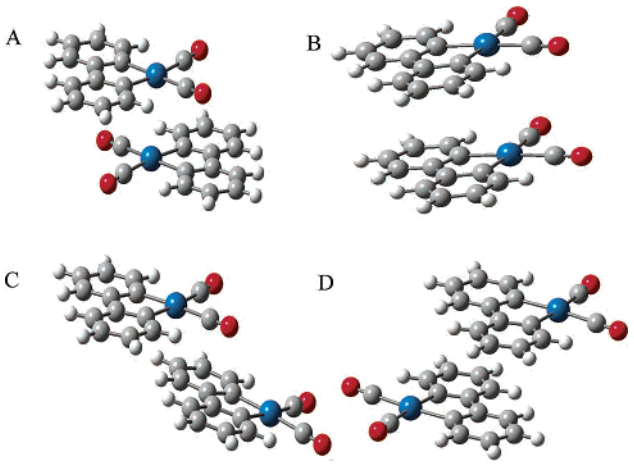

Figure 2. Optimized structures of the proposed dimers of [Pt(bph)(CO)$_2$] calculated using B3LYP theory and the 6-311G** basis set on the C, O, and H atoms and the SDD ECP on the Pt atom: (A) dimer **A**; (B) dimer **B**; (C) dimer **C** (CO above bph); (D) dimer **D** (bph above bph).

dimer **D**. For all dimers the Pt−Pt distance was initially set to 3.24 Å as found experimentally. In dimer **C** one of the monomers was translated by 5.00 Å along the *y* axis relative to dimer **B**. In dimer **D** one of the monomers was translated by 5.0 Å along the *y* axis relative to dimer **A**. The input geometry of the trimer was prepared by addition of a monomer unit to dimer **A** (Figure 1C). The Pt1−Pt2−Pt3 angle was set initially to 180°, and C1′−Pt2−Pt3−C1″ was set to 180°. All geometry parameters for the trimer were further optimized (Table 1).

Dimers **B**, **C**, and **D** were optimized in C_1 symmetry (Figure 2). A grid of 75 radial shells and 302 angular points per shell was used for numerical integrations of the two-electron integrals and their derivatives.[25] The tolerance limits for both distance and nondistance comparisons for the molecular symmetry determination were set to 10^{-4}. The values of the spin contamination $\langle S^2 \rangle$ of the Kohn−Sham determinants were 2.02 for the triplet monomer and 2.01 for the triplet dimer **A**. Thus, the effect of the spin contamination should be small.

The atomic orbital coefficients were calculated using Mulliken population analysis. The atomic orbital contributions for monomer, expressed in percent, are given in Table 2A and those for the dimer **A** in Table 2B. Percent contributions were calculated using eq 1, where n is the atomic orbital coefficient and $\sum n^2$ is the sum of the squares of all atomic orbital coefficients in a specific molecular orbital.

$$[n^2/\sum n^2] \times 100 = \%\ \text{contribution} \qquad (1)$$

The percent contributions are calculated per C and O atoms of one CO ligand. For the biphenyl dianion the sum of the percent contributions for six carbon atoms of one phenyl ring is given. Hydrogen atom contributions are generally small and are not presented.

Singlet excited states were calculated based on the singlet ground-state geometry, whereas triplet excited states were calculated based on the lowest-lying triplet-state geometry, both utilizing the direct TDDFT.[26−28] The output contained information for the symmetries of the transitions giving rise to the excited states and the orbitals involved with the orbital coefficient of the transition. The symmetry of a vertical transition is determined according to eq 2,[29]

$$(\Gamma\psi_o)\,(\Gamma_{op})\,(\Gamma\psi_v) = \Gamma \qquad (2)$$

where $\Gamma\psi_o$ and $\Gamma\psi_v$ are the orbital symmetries of the occupied (ψ_o) and the virtual (ψ_v) orbitals and Γ_{op} is the symmetry of the optical transition $\psi_o \rightarrow \psi_v$. Γ would be A_1 and A_g for the C_{2v} and C_{2h} point groups, respectively. The energy of each excited state as well as the value of its oscillator strength is also tabulated. Data for the singlet and triplet excited states of the monomer and dimer **A** are given in Table 3, parts A and B, respectively.

Each excited state was simulated with a Gaussian curve. The singlet excited states that appear in Table 3A were fit to Gaussian line shapes with maxima equal to the molar absorptivity. The results for the monomer are illustrated in Figure 3A and for dimer **A** in Figure 3B. The line with ×'s gives the sum of all Gaussian peaks. The oscillator strength f is related to the molar absorptivity coefficient ϵ through eq 3. The integration is over the entire band (ω is the frequency in cm^{-1}), and F is related to the solvent refractive index. For the most common solvents F is close to unity.[30] As a crude but convenient approximation, we used eq 4 to convert f to ϵ. The full-width at half-maximum $\Delta\omega_{1/2}$ (cm^{-1}) was estimated to be 970 cm^{-1} from the most well-defined and narrowest peak in the absorption spectrum (at 281 nm) of [Pt(bph)(CO)$_2$] in CH_2Cl_2,[6] assuming that it was due to a single electronic transition.

$$f = (4.32 \times 10^{-9})F\int_{\omega_1}^{\omega_2} \epsilon\, d\omega \qquad (3)$$

$$f = (4.32 \times 10^{-9})(\epsilon_{max})(\Delta\omega_{1/2}) \qquad (4)$$

(25) Trucks, G. W.; Frisch, M. J. Rotational Invariance Properties of Pruned Grids for Numerical Integration. In preparation, 1998.
(26) Stratmann, R. E.; Scuseria, G. E.; Frisch, M. J. *J. Chem. Phys.*, submitted for publication, 1998.
(27) Bauernschmitt, R.; Ahlrichs, R. *Chem. Phys. Lett.* **1996**, *256*, 454.
(28) Casida, M. E.; Jamorski, C.; Casida, K. C.; Salahub, D. R. *J. Chem. Phys.* **1998**, *108*, 4439.

Table 2. The Percent Molecular Orbital Populations for (A) the Monomer and (B) Dimer **A** of [Pt(bph)(CO)$_2$] in the Singlet Ground State[a]

		Pt									C(1)	O	C[b]	
molecular orbital	E, eV	s	p_x	p_y	p_z	d_{z^2}	d_{xz}	d_{yz}	$d_{x^2-y^2}$	d_{xy}	$\Sigma_{s,p,d}$	$\Sigma_{s,p,d}$	$\Sigma_{s,p,d}$	type
						(A) Monomer								
59 (O), B_1	−7.69	0	0.3	0	0	0	5.2	0	0	0	0	0.2	46.8	bph
60 (O), A_1	−7.52	34.6	0	0	2.6	8.5	0	0	20.4	0	2.2	0.2	13.7	$Pt_{s,d}$
61 (O), B_1	−6.90	0	3.0	0	0	0	11.3	0	0	0	0.8	1.6	40.2	bph
62 (O), A_2	−6.65	0	0	0	0	0	0	0	0	9.6	0.2	0.2	44.5	bph
63 (O), A_2	−5.83	0	0	0	0	0	0	0	0	5.2	0.2	0.2	46.6	bph
64 (V), B_1	−2.65	0	18.9	0	0	0	9.0	0	0	0	15.4	11.6	8.8	$Pt_{p,d}$, CO
65 (V), B_2	−1.42	0	0	3.2	0	0	0	0.2	0	0	17.4	8.4	21.9	CO, bph
66 (V), A_1	−1.41	0.8	0	0	1.2	10.0	0	0	4.2	0	22.2	10.7	8.2	CO
67 (V), A_2	−1.17	0	0	0	0	0	0	0	0	10.8	27.7	14.6	2.3	CO
68 (V), B_1	−0.90	0	0.3	0	0	0	1.0	0	0	0	1.2	0.6	47.1	bph
69 (V), B_2	−0.34	0	0	12.3	0	0	0	28.6	0	0	4.3	2.4	18.9	Pt_d
70 (V), B_1	−0.24	0	1.1	0	0	0	7.0	0	0	0	3.9	1.9	40.0	bph
						(B) Dimer **A**								
112 (O), B_g	−8.81	0	0	0	0.5	0	41.1	37.9	0	0	0.8	2.0	7.1	Pt_d
113 (O), A_g	−8.55	4.8	0.2	1.4	0	24.3	0	0	2.3	46.6	2.7	0.9	6.2	Pt_d
114 (O), A_u	−8.47	0	0	0	4.7	0	6.1	11.7	0	0	10.0	0.8	24.5	Pt_d, bph
115 (O), B_u	−8.39	2.0	2.1	2.6	0	15.4	0	0	2.1	15.6	7.5	1.1	19.9	Pt_d
116 (O), B_g	−8.36	0	0	0	4.7	0	19.1	2.8	0	0	10.2	0.9	23.0	Pt_d, bph
117 (O), A_g	−7.88	28.5	2.3	2.4	0	0.8	0	0	0.4	7.4	5.3	0.5	22.2	Pt_s
118 (O), A_g	−7.77	7.4	0.9	0.7	0	0.5	0	0	6.9	0.6	0.9	0.2	40.1	bph
119 (O), B_u	−7.74	2.1	0.5	0.2	0	0.2	0	0	6.6	0.3	0.1	0.2	44.8	bph
120 (O), B_u	−7.07	24.4	2.0	2.2	0	7.8	0	0	9.1	19.6	0.7	0.6	15.8	$Pt_{s,d}$
121 (O), A_g	−7.03	2.2	2.7	1.4	0	0.6	0	0	13.7	0.3	1.1	2.1	36.3	Pt_d, bph
122 (O), A_u	−6.72	0	0	0	0	0	7.5	4.0	0	0	0.2	0.1	43.8	bph
123 (O), B_g	−6.71	0	0	0	0.2	0	6.6	3.2	0	0	0.3	0.4	44.3	bph
124 (O), B_u	−6.67	21.9	1.4	0.6	0	6.5	0	0	1.8	26.5	0.2	0.1	20.2	$Pt_{s,d}$
125 (O), B_g	−5.92	0	0	0	0.8	0	3.3	1.6	0	0	0.4	0.4	46.3	bph
126 (O), A_u	−5.87	0	0	0	0.2	0	4.9	2.7	0	0	0.2	0.1	45.7	bph
127 (V), A_g	−2.76	5.7	17.6	4.8	0	0.8	0	0	4.9	2.4	11.6	8.3	12.0	Pt_p, CO
128 (V), B_u	−2.01	7.1	9.9	4.5	0	1.0	0	0	7.6	0.4	16.4	10.7	7.6	$Pt_{p,d}$, CO
129 (V), B_u	−1.26	1.1	0.5	0.7	0	9.6	0	0	0.1	2.8	21.0	10.0	11.0	CO
130 (V), A_g	−1.25	2.0	0.3	1.9	0	10.0	0	0	0.3	2.8	20.2	9.9	10.8	CO
131 (V), A_u	−1.23	0	0	0	4.0	0	0.1	0.2	0	0	17.3	8.4	21.7	CO, bph
132 (V), B_g	−1.20	0	0	0	5.5	0	0	0.4	0	0	17.0	8.1	21.5	CO, bph
133 (V), B_g	−1.00	0	0	0	0.2	0	2.0	7.4	0	0	24.0	12.4	8.6	CO
134 (V), A_g	−0.98	3.6	0.8	2.4	0	0.8	0	0	0.6	0.8	2.1	0.9	42.4	bph
135 (V), A_u	−0.95	0	0	0	0.9	0	5.0	5.5	0	0	26.6	13.4	3.9	CO
136 (V), B_u	−0.93	1.6	0.3	0.1	0	2.0	0	0	1.6	0.2	5.6	2.3	39.1	bph
137 (V), B_u	−0.31	43.1	2.5	3.5	0	0.1	0	0	2.9	0.4	1.3	0.7	21.8	Pt_s
138 (V), A_u	−0.24	0	0	0	15.2	0	10.7	15.2	0	0	4.9	1.6	18.1	$Pt_{p,d}$
139 (V), B_g	−0.23	0	0	0	24.4	0	8.4	18.6	0	0	3.5	2.0	16.6	$Pt_{p,d}$

[a] The orbital occupancy status is given in parentheses (O = occupied, V = virtual), followed by the orbital symmetry. Type describes the moiety with the largest share in the spatial distribution of the orbital. For example, Pt_d means electron density is located on the d orbitals of Pt. (See text for calculation details.) [b] Sum of the percent populations for the six carbon atoms of one phenyl.

Similarly, five triplet excited states of dimer **A** were simulated by Gaussian curves (vide infra).

Discussion

Dimer Formation. The square planar neutral complexes of Pt(II) containing planar ligands are known to often crystallize in one-dimensional polymers featuring equal Pt−Pt distances along the polymer chain. As a result of the interaction between ligands from different complexes, the angle of rotation of successive stacked complexes about the Pt−Pt bond when viewed down the chain axis is close to 180°. We investigated the singlet ground-state energies of four dimers (Figure 2) of [Pt(bph)(CO)$_2$] and compared them to E_o defined as twice the singlet ground-state energy of the monomer in C_{2v} symmetry.

The lowest energy dimer **A** (Figure 2A) was similar to the one reported in the single crystal of the complex (Table 1).[24] It was stabilized by $\pi-\pi$ interactions between the aromatic and the carbonyl systems as well as by Pt−Pt binding. The energy of dimer **A** was 4.09 kcal/mol lower than E_o. Geometry optimization for dimer **B** (Figure 2B) converged at a Pt−Pt distance of 6.07 Å with an energy slightly higher than E_o (by ca. 1.03×10^{-3} kcal/mol). Apparently, there is no $\pi-\pi$ attraction between ligands of the same kind but repulsion. Dimer **C** has a small binding energy (1.90 kcal/mol lower than E_o). The approximate planes of the two biphenyl groups of the monomers were not parallel (Figure 2C) possibly enhancing the effect of the $\pi-\pi$ interactions. The energy of dimer **D** was higher than E_o by 1.96 kcal/mol, and the distance between C7 of two different monomers was 4.19 Å (Figure 2D). The anticipated $\pi-\pi$ interaction between the two biphenyl groups did not lead to lower energy.

The preferred stacking modes of [Pt(bph)(CO)$_2$] can be justified not only by the Pt−Pt binding and the biphenyl−

(29) Drago, R. S. *Physical Methods for Chemists*, 2nd ed.; Saunders College Publishing: Ft. Worth, FL, 1977; p 123.
(30) Horvath, O.; Stevenson, K. L. *Charge Transfer Photochemistry of Coordination Compounds*; VCH Publishers: New York, 1993; pp 10−12.

Table 3. Calculated Singlet and Triplet Excited States of the Monomer and Dimer **A** of $[Pt(bph)(CO)_2]$[a]

(A) Singlet

state	Γ_{op}	E_{VER}, eV	f	$\psi_o \rightarrow \psi_v$	type
			Monomer		
2	B_2	3.39	0.039	62 → 64 (0.7)	LMLCT
3	A_1	3.70	0.102	61 → 64 (0.6)	LMLCT
6	B_1	3.96	0.019	60 → 64 (0.7)	MMLCT
7	A_1	4.07	0.047	63 → 67 (0.7)	LLCT
8	A_1	4.44	0.029	59 → 64 (0.7)	LMLCT
9	B_2	4.50	0.300	63 → 68 (0.6)	$\pi \rightarrow \pi^*$
15	B_2	4.79	0.012	63 → 70 (0.6)	$\pi \rightarrow \pi^*$
20	B_2	5.03	0.016	60 → 65 (0.6)	MLCT
			Dimer **A**		
5	B_u	3.29	0.252	124 → 127 (0.7)	MMLCT
7	A_u	3.38	0.043	122 → 127 (0.7)	LMLCT
8	B_u	3.68	0.075	120 → 127 (0.7)	MMLCT
21	B_u	4.23	0.046	126 → 133 (0.7)	LLCT
25	B_u	4.33	0.010	125 → 135 (0.6)	LLCT
28	A_u	4.47	0.175	126 → 134 (0.6)	$\pi \rightarrow \pi^*$
30	B_u	4.48	0.094	121 → 128 (0.5)	LMLCT
34	B_u	4.56	0.016	124 → 130 (0.6)	MLCT
35	A_u	4.56	0.298	125 → 136 (0.6)	$\pi \rightarrow \pi^*$
38	A_u	4.75	0.021	115 → 127 (0.4)	Pt centered
				126 → 139 (0.4)	LMCT
39	A_u	4.76	0.011	122 → 130 (0.4)	LLCT
				123 → 129 (0.4)	LLCT

(B) Triplet

state	Γ_{op}	E_{VER}, eV	f	$\psi_o \rightarrow \psi_v$	type
			Monomer		
1	A_1	1.24	0.021	64A → 65A (0.8)	Pt → del[b]
3	A_1	1.60	0.045	62B → 63B (0.8)	$\pi \rightarrow \pi^*$
7	B_2	2.10	0.012	64A → 66A (0.9)	$\pi \rightarrow \pi^*$
9	A_1	2.21	0.046	64A → 69A (1.0)	MLCT
11	B_2	2.66	0.053	64A → 70A (0.8)	MLCT
14	B_1	3.08	0.015	64A → 72A (1.0)	Pt centered
15	B_2	3.24	0.040	64A → 73A (0.8)	MLCT
16	A_1	3.32	0.020	56B → 63B (1.0)	MLCT
17	B_2	3.38	0.016	55B → 63B (0.8)	MLCT
19	B_2	3.73	0.035	62B → 64B (0.8)	LMLCT
			Dimer **A**		
7	B_u	1.30	0.156	127A → 128A (0.9)	Pt, CO → del[b]
9	B_u	1.72	0.029	127A → 130A (0.9)	Pt, CO → del[b]
14	B_u	1.92	0.010	127A → 134A (0.9)	MLCT
17	A_u	2.14	0.038	117B → 126B (0.8)	MLCT
19	A_u	2.22	0.034	127A → 136A (0.9)	MLCT
21	B_u	2.46	0.053	127A → 137A (0.8)	Pt centered
29	B_u	2.86	0.031	112B → 126B (1.0)	MLCT
31	B_u	2.98	0.156	124B → 127B (1.0)	Pt centered
32	A_u	3.02	0.022	125B → 128B (0.7)	LMLCT
40	B_u	3.39	0.017	127A → 144A (1.0)	Pt centered

[a] Γ_{op} is the symmetry of the excited state (eq 1), E_{VER} is the energy of the vertical transition, f is the oscillator strength, ψ_o and ψ_v are the occupied and the virtual orbitals that define the transition, and the transition type is determined based on the change in the spatial distribution from occupied to virtual orbital. The orbital coefficient for each transition is given in parentheses. (See text for calculation details.) [b] Del = delocalized.

carbonyl $\pi-\pi$ interaction but also by the calculated atomic charges in the complex. The negative charge of −0.28 on C2 and the positive charge of +0.11 on C1 stabilize dimer **A** by electrostatic attraction when the two charged atoms are close in space. The above interpretation would discredit dimer **B**, where the electrostatic biphenyl−biphenyl and carbonyl−carbonyl repulsions on adjacent $[Pt(bph)(CO)_2]$ molecules would prevent stacking. It is likely that the negative charge on the O atom (−0.16) may contribute to the acute angle between the approximate planes of the two monomers in dimer **C**. On the basis of the above results, we would consider dimers **B**, **C**, and **D** as local minima not likely to make major contributions to aggregation and will further describe the electronic excited states of dimer **A** only.

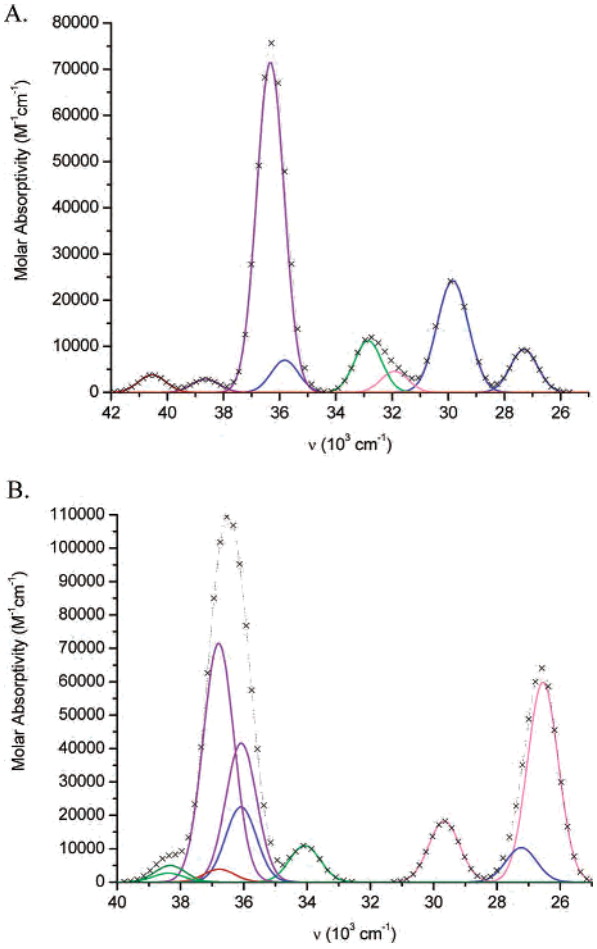

Figure 3. Calculated spectra of $[Pt(bph)(CO)_2]$ based on Gaussian curve fits for every singlet excited state from Table 3A (based on the singlet ground state) in wavenumber versus molar absorptivity: (A) monomer; (B) dimer **A**. Line colors: LMLCT, blue; LLCT, green; MMLCT, light magenta; $\pi \rightarrow \pi^*$, purple; MLCT, red; Pt centered, olive; sum, black (with ×'s).

Singlet Geometry Optimization. The results of computations for the singlet monomer, dimer **A**, and the trimer of $[Pt(bph)(CO)_2]$ are listed in Table 1 together with selected structural properties from the X-ray crystallographic report.[24] Good agreement between calculation and experiment was achieved for the C2−Pt−C2′ and C1−Pt−C1′ angles. The calculated Pt−C1 and Pt−C2 bond distances were slightly longer than those found experimentally. The calculated Pt−Pt distance for dimer **A** was about 7% longer than that found experimentally. The bond distances calculated for C1−O and C7−C7′ were outside the error limits determined using X-ray crystallography.

In dimer **A** the two monomers were distorted from planarity to accommodate Pt−Pt binding. The torsion angle C1−Pt−C1′−C2 changed from 180.0° for the monomer (Figure 1A) to 156.6° for dimer **A** displacing the ligands that belong to different monomers apart and bringing the two Pt atoms closer together. The Pt−Pt−Pt angle obtained from geometry optimization of the trimer was in excellent agreement with the X-ray result. These results obtained with one of the largest basis sets appear satisfactory despite the

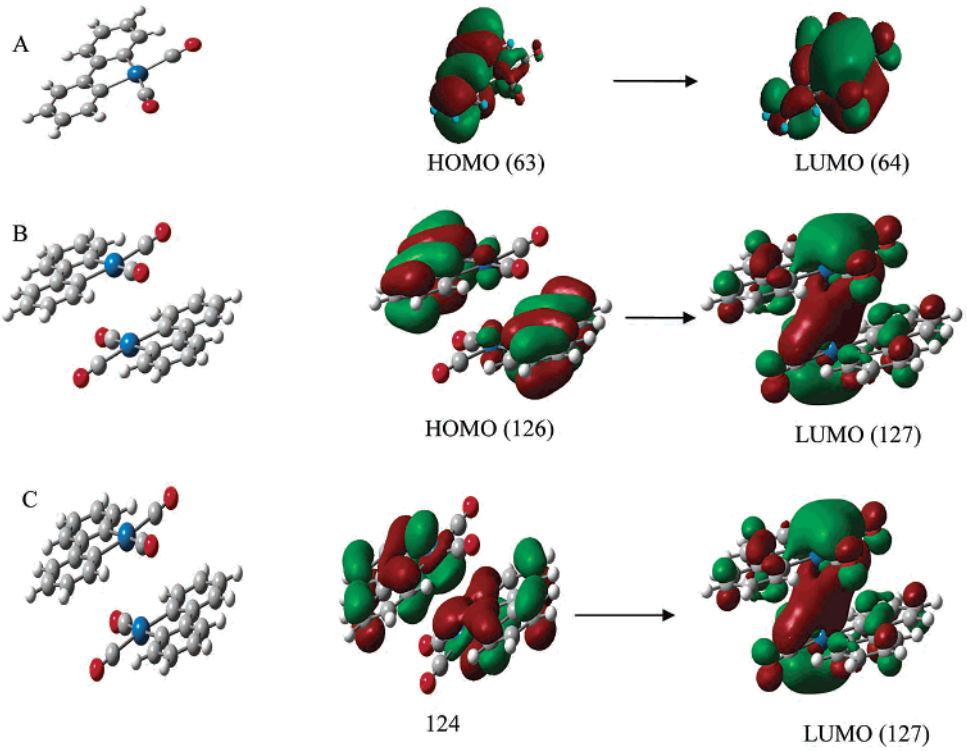

Figure 4. Molecular orbital schemes of electronic transitions that involve the monomer and dimer **A** calculated using B3LYP theory and the 6-311G** basis set on the C, O, and H atoms and the SDD ECP on the Pt atom: (A) lowest energy transition for the monomer; (B) lowest energy transition for dimer **A**; (C) transition that gives rise to singlet excited state 5 for dimer **A**.

reported shortcomings associated with calculations of metal−ligand bond distances using B3LYP theory.[31,32]

Triplet Geometry Optimization. The lowest-lying triplet-state geometries of the monomer, dimer **A**, and the trimer (Table 1) were found to differ from those in the singlet ground state. Both the Pt−C1 and Pt−C2 bond lengths were shorter by about 0.01 Å in the triplet state compared to the bond lengths in the singlet ground state. The Pt−Pt distance in dimer **A** was 3.34 Å in the triplet state but 3.48 Å in the singlet ground state. This represents a relative shrinkage of roughly 4.0% for the Pt−Pt distance. The latter value was close to the one determined using polarized absorption and emission spectroscopy of a single crystal of $K_4[Pt_2(H_2P_2O_5)_2]$ (shrinkage of ca. 7%).[33,34]

The chain of the complex was straighter in the lowest-lying triplet state than in the singlet ground state (the Pt1−Pt2−Pt3 angle in the triplet trimer was significantly larger than that in the singlet ground state of the trimer), which may result from the shorter Pt−Pt bond distances. In the optimized structure of the lowest-lying triplet state of the trimer in C_s symmetry, two adjacent monomers were in closer proximity whereas the third was more distant. The difference between the two Pt−Pt distances was about 0.01 Å; however, this was not observed for the singlet ground state of the trimer. We can extrapolate this result to longer linear polymers as before[3] and note that in the lowest-lying triplet state, the most stable species in linear chains of $[Pt(bph)(CO)_2]$ would be the triplet dimer **A**.

Molecular Orbital Analysis. The energies and the percent molecular orbital contributions for the monomer and dimer **A** of $[Pt(bph)(CO)_2]$ in the singlet ground state are listed in Table 2. For the monomer (Table 2A) the highest occupied molecular orbital (HOMO) is located on the biphenyl ligand p_x orbitals (ca. 93% overall) and the lowest unoccupied molecular orbital (LUMO) is located on the Pt p_x (ca. 19%), Pt d_{xz} (ca. 9%), and carbonyl ligand p_x orbitals (ca. 54% overall). These orbitals are shown in Figure 4A. Occupied orbital 60 features roughly 66% metallic antibonding character, and orbitals 59, 61, and 62 are strongly delocalized over the biphenyl moiety. Virtual orbitals 66 and 67 are substantially carbonyl centered and have significant metal contributions. Orbital 65 is strongly delocalized. The fifth and the seventh virtual orbitals (68 and 70) are predominantly delocalized on biphenyl (ca. 94% and 80%, respectively).

The energies of 13 virtual and 15 occupied orbitals of dimer **A** are listed in Table 2B together with the moieties that make the most significant contributions to the orbitals. Generally, the frontier orbital spatial distributions in dimer **A** are slightly perturbed from those of the monomer. The low-energy occupied orbitals 112−121 are essentially metal centered except for 118 and 119 that are biphenyl centered. Orbital 112 is calculated to have roughly 79% Pt_d orbital contribution. More than 87% of biphenyl character is reported for the two pairs of degenerate occupied orbitals 122, 123 and 125, 126 (HOMO). The latter has a spatial distribution similar to that of the monomer HOMO. Orbital 124 is

(31) Buchs, M.; Daul, C. *Chimia* **1998**, *52*, 163−166.
(32) Stoyanov, S. R.; Villegas, J. M.; Rillema, D. P. *Inorg. Chem.* **2002**, *41*, 2941−2945.
(33) Rice, S. F.; Gray, H. B. *J. Am. Chem. Soc.* **1983**, *105*, 4571−4575.
(34) Bär, L.; Gliemann, G. *Chem. Phys. Lett.* **1984**, *108*, 14.

classified as Pt antibonding (Figure 4). The antibonding character is determined based on a visual examination of the spatial distributions of the α and β electrons. The LUMO of dimer **A** has a significantly higher metal contribution relative to the LUMO of the monomer, 22.4% from p and 13.7% from s and d orbitals of Pt, and the carbonyl part is of π^* character. The HOMO and the LUMO of dimer **A** are shown in Figure 4B. The energy difference between the HOMO and the LUMO in dimer **A** is 3.12 eV compared to 3.18 eV for the monomer. Virtual orbitals 129−136 are antibonding and ligand π^* centered.

Singlet Excited States. Contrary to the classical treatment of vertical one-electron excitation, the excited states calculated through TDDFT are described in terms of combinations of several transitions from occupied to virtual molecular orbitals. Twenty singlet excited states were produced by the TD routine of DFT in the energy ranges of the absorption and excitation spectra for the monomer, and twice as many excited states were obtained for dimer **A** of [Pt(bph)$(CO)_2$] based on $^1A_1$ and ^1A_g ground-state geometries, respectively. Only excited states generated from lower energy states with oscillator strengths of >0.01 for the monomer and the dimer **A** are listed in Table 3A. The energies of the singlet excited states range from 3.29 to 5.03 eV.

Excited states that arise from transitions between orbitals that were located on different moieties were classified as charge transfer (CT) excited states. Those from π-occupied to π-virtual orbitals located on the same ligand were described as $\pi \rightarrow \pi^*$ states, but those from orbitals on different ligands were described as ligand-to-ligand charge transfer (LLCT) states. Metal-to-ligand charge transfer (MLCT) states involve transitions from the metal atom to ligand-centered orbitals, whereas in metal-to-metal−ligand charge transfer (MMLCT) excited states, the virtual orbital is located on the metal and on one of the ligands. The excited state was platinum centered if the orbitals involved in the transition were primarily located on the Pt atom.

Only the most significant transitions associated with each excited state are listed in Table 3. For example, for excited state 8 at 4.44 eV two transitions are calculated: $59 \rightarrow 64$ with an orbital coefficient of 0.68 and $61 \rightarrow 68$ with an orbital coefficient of 0.10. Only the first transition is listed in Table 3A as it has a significantly larger absolute value of the orbital coefficient. If multiple transitions have orbital coefficients with absolute values that differ from the largest one by less than 0.2, they are listed, for example, excited states 38 and 39 for dimer **A** in Table 3A. The subsequent discussion is related to the predicted excited-state transitions in order to correlate them with experimental spectra.

Three singlet excited states of A_1, four of B_2, and one of B_1 symmetry were found with vertical transition energies (E_{VER}) in the UV−vis region for the monomer. Excited state 9 located at about 280 nm was the most intense and resulted from a $\pi \rightarrow \pi^*$ transition.[6] Excited state 3 at 3.70 eV featured about one-third of the oscillator strength of excited state 9 and arose from a transition from the biphenyl ligand (HOMO-2) to the state consisting of the p and d orbitals of Pt and the π^* orbitals of CO (LUMO). This transition is labeled as a ligand-to-metal−ligand charge transfer (LMLCT) transition, not as a MLCT transition.[6] These two states represented the most intense peaks in the simulated singlet excited-state spectrum of the complex (vide infra).

In the same energy range (from 0 to 5 eV) dimer **A** featured five A_u and six B_u singlet excited states. The oscillator strength of excited state 35 (A_u) derived from a $\pi \rightarrow \pi^*$ transition was close in energy and similar in type to the formation of excited state 9 of the monomer. The first of the two degenerate states 28 and 30 was also derived from a $\pi \rightarrow \pi^*$ transition, but the second resulted from a transition from biphenyl to CO (LLCT). Excited state 8 arose from an MMLCT state, similar to the experimentally based assignment[6] for the transition at about 330 nm. The second most intense excited state 5 was populated from the $Pt_{s,d}$ centered antibonding orbital 124 (ca. 71% on the metal atom) to the Pt/CO(π^*) centered LUMO (orbital 127).

Different assignments have been presented in the literature for the lowest energy transition of [Pt(bph)$(CO)_2$] in the solid state. Generally, it has been assigned as a metal-centered transition with the HOMO on the dσ^* orbitals of Pt, but the LUMO has been placed on p_x(Pt)/π^*(CO)[3,5,35] (for axes assignments see Figure 1A) or on pσ[36,37] depending on the theory employed. This is similar to the result presented for the lowest energy singlet excited state of dimer **A**, based on the excitation from orbital 124 to the LUMO (Figure 4C). Occupied orbital 124 is d_{xy} antibonding, and the LUMO spatial distribution (orbital 127) is in agreement with the description as Pt p_x and CO π^*. Excited state 6 of the monomer also fits the above description but the oscillator strength associated with its formation is 1 order of magnitude lower.

Simulated Spectra. Each excited state listed in Table 3A was fit to a Gaussian curve, and the areas below the curves were added to produce the sum curve (Figure 3A for the monomer and Figure 3B for dimer **A**). The curves are colored based on the assignments of the excited states in Table 3A. The successful simulation of the spectra is strongly dependent on the proper selection of $\Delta\omega_{1/2}$ which affects the value of ϵ. If the full-width at half-maximum is larger, the Gaussian curves broaden and spread along the energy axis and the molar absorptivity is lower.

The absorption spectrum of [Pt(bph)$(CO)_2$] in CH_2Cl_2 is reprinted from ref 6 for comparison and overlaid with the simulated spectra based on singlet excited states for the monomer and dimer **A** (Figure 5). Only the excited states that arise from singlet−singlet transitions were correlated with the UV−vis spectrum. The estimate of the integral area below the sum simulated spectra shown in Figure 3, parts A and B, for both the monomer and dimer **A** per metal atom is very close to the one measured in CH_2Cl_2. The shift of some of the calculated peaks compared to the experimental ones is due to solvent effects. All calculations were done in

(35) Hidvegi, I.; von Ammon, W.; Gliemann, G. *J. Chem. Phys.* **1982**, *76*, 4361−4369.
(36) Krogmann, K. *Angew. Chem., Int. Ed. Engl.* **1969**, *8*, 35−42.
(37) Roundhill, R. D.; Gray, H. B.; Che, C.-M. *Acc. Chem. Res.* **1989**, *22*, 55−61.

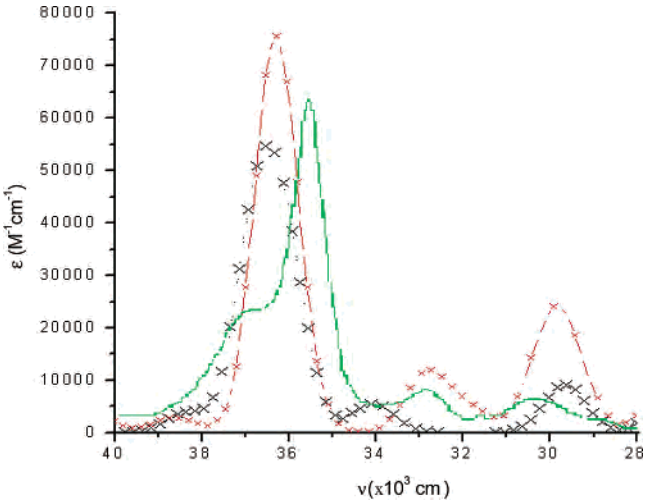

Figure 5. Overlay of the experimental absorption spectrum of [Pt(bph)(CO)$_2$] (green, solid line) in CH_2Cl_2 (data from *Inorg. Chem.* **1998**, *37*, 1392−1397) and the simulated absorption spectra of the monomer (red, dashed line with ×'s) and dimer **A** (black, dotted line with ×'s). The molar absorptivity of the latter is given per metal atom.

Table 4. Experimental Absorption Energies ($\times 10^3$ cm^{-1}) and B3LYP/TDDFT Calculated Singlet Excited-State Energies ($\times 10^3$ cm^{-1}) for the Monomer and Dimer **A** of [Pt(bph)(CO)$_2$][a]

absorption in CH_2Cl_2	singlet monomer	singlet dimer **A**
37.0	36.3 (0.7)	36.8 (0.2)
35.6	35.8 (0.2)	36.1 (0.5)
32.9	32.8 (0.1)	34.1 (1.2)
30.3	29.8 (0.5)	29.7 (0.6)

[a] The value of the absolute deviation of the calculated energy compared to the experimental energy in CH_2Cl_2 is given in parentheses.

the gas phase. The molar absorptivity at roughly 36 250 cm^{-1} was simulated to be about 75 640 M^{-1} cm^{-1} compared to 64 600 M^{-1} cm^{-1} found experimentally. The simulated peak at 33 000 cm^{-1} featured $\epsilon = 11\,910$ M^{-1} cm^{-1} compared to the experimental $\epsilon = 10\,400$ M^{-1} cm^{-1}. The LMLCT peak at 30 000 cm^{-1} (calculated $\epsilon = 24\,090$ M^{-1} cm^{-1}) was about 4 times more intense compared to the experimental one ($\epsilon = 5910$ M^{-1} cm^{-1}). For the dimer **A** per metal center simulation, the prominent maximum at 36 250 cm^{-1} would then have $\epsilon = 55\,000$ M^{-1} cm^{-1} and the excitation at 29 700 cm^{-1} would be only 1.5 times more intense than the experimental value in CH_2Cl_2. However, the intense peak predicted at 26 250 cm^{-1} is not present in the experimental spectrum.

The calculated excited-state energies and the absorption spectrum peak energies in CH_2Cl_2 are listed in Table 4, and the absolute deviations of the simulated spectra for the monomer and dimer **A** are shown in parentheses. The deviations for both the monomer and dimer **A** are within the average error of 890 cm^{-1} reported previously for 86 experimental triplet−triplet absorption energies calculated with TDDFT, and the singlet−singlet energies obtained were less accurate.[17] Upon increasing the concentration of [Pt(bph)(CO)$_2$] in solution and surpassing the limiting concentration of aggregation, the absorption spectrum converts from that of the monomer to that of dimer **A**. Generally, the simulation reproduces the energies and the intensities of the major experimental peaks quite well.

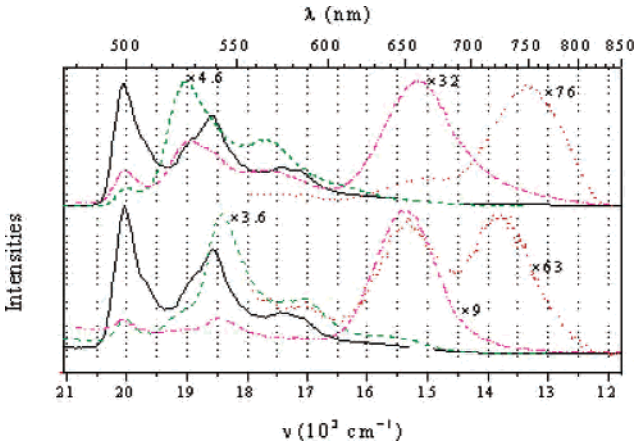

Figure 6. Experimental emission spectra of [Pt(bph)(CO)$_2$]: (top) in concentrated solutions of 4:1 (v/v) C_2H_5OH/CH_3OH excited at 330 nm (—), 393 nm (- - -), 436 nm (-·-), and 501 nm (···); (bottom) in concentrated solutions of 4:1 (v/v) MeTHF/CH_2Cl_2 excited at 330 nm (—), 390 nm (- - -), 434 nm (-·-), and 501 nm (···). Adapted from *Inor. Chem.* **1998**, *37*, 1392−1397.

Triplet Excited States. Triplet excited states were calculated, 20 for the monomer and 40 for the dimer **A**, based on the lowest-lying triplet-state geometries, $^3B_2$ for the monomer and ^3A_u for dimer **A**. The energies of the triplet excited states ranged from 1.24 to 3.73 eV. The states with $f > 0.01$ are listed in Table 3B. Generally, the oscillator strengths for triplet excited state formation of the monomer were about 5 times lower than those of the singlet excited states. Five of the most intense excited states 9, 11, and 15−17 were MLCT states. Excited states 3 and 7 were derived from $\pi \rightarrow \pi^*$ transitions, and excited state 19 was derived from a ligand-to-metal−ligand charge transfer state. Most triplet excited states were based on excitation from the α HOMO (64A). The excited states of the dimer **A** arose from MLCT transitions. The most intense triplet excited states of the dimer were also associated with excitation from the α HOMO (127A). The triplet excited states of the trimer were very close in energy and lower in oscillator strength relative to those of the triplet dimer.

Low-Energy Excitation and Emission Analysis. In the experimental excitation spectrum[6] there are low-energy peaks (<30 000 cm^{-1}) that can be linked to the emission and the calculated triplet excited states of the monomer and dimer **A** of the complex. In concentrated solutions of [Pt(bph)(CO)$_2$] in 4:1 (v/v) MeTHF/CH_2Cl_2 and 4:1 (v/v) C_2H_5OH/CH_3OH (Figure 6) there are four major emission peaks due to excitations at different energies. The emission lifetime of [Pt(bph)(CO)$_2$] in 4:1 (v/v) C_2H_5OH/CH_3OH at 298 K was 2.2 μs upon excitation at 506, 544, or 590 nm, and the emission was attributed to a triplet biphenyl-centered excited state.[6] Only triplet excited-state energies calculated from the lowest-lying triplet state were correlated to the experimental emission energies. Experimental low-energy excitation and emission energies as well as triplet excited-state energies for the monomer and dimer **A** are listed in Table 5, and the absolute deviations are given in parentheses. The higher excitation energies of the monomer were found to deviate by 700 cm^{-1} or less from the experimentally based values in the two solvent systems. The triplet excited states of dimer

Table 5. Experimental Excitation and Emission Energies ($\times 10^3$ cm^{-1}) and B3LYP/TDDFT Calculated Triplet Excited-State Energies ($\times 10^3$ cm^{-1}) for the Monomer and Dimer **A** of [Pt(bph)(CO)$_2$][a]

excitation	emission	triplet monomer	triplet dimer **A**
	(A) Excitation and Emission in 4:1 (v/v) MeTHF/CH_2Cl_2		
27.5		27.2 (0.3)	27.3 (0.2)
25.6		26.1 (0.5)	24.3 (1.3)
23.0			23.2 (0.2)
20.0	20.0	21.4 (1.4)	19.8 (0.2)
	18.4	17.8 (0.6)	17.9 (0.5)
	17.1	16.9 (0.2)	17.3 (0.2)
	15.3		15.5 (0.2)
	13.8	12.9 (0.9)	13.9 (0.1)
	(B) Excitation and Emission in 4:1 (v/v) C_2H_5OH/CH_3OH		
27.5		27.2 (0.3)	27.3 (0.2)
25.4		24.8 (0.6)	24.3 (1.1)
22.9			23.2 (0.3)
20.0	20.0	21.4 (1.4)	19.8 (0.2)
	17.7	16.9 (0.8)	17.9 (0.2)
	15.2	-	15.5 (0.3)
	13.3	12.9 (0.4)	13.9 (0.6)

[a] The value of the absolute deviation of the calculated energy compared to the experimental energy is given relative to excitation and emission energies.

A at high energy were not in a good agreement with the experimental excitation spectrum. However, the lower energy peaks (23 000 cm^{-1} and below) were better-reproduced by the dimer **A** excited states.

The emission peaks on the other hand were best correlated with the triplet excited states of the dimer. The largest deviation relative to the alcohol solvent system was 600 and 500 cm^{-1} relative to the other solvent system. The rest of the excited states were within 200 cm^{-1} of the experimental values. These errors were smaller than reported elsewere.[17]

For dimer **A** the most intense peak located at 20 000 cm^{-1} (metal centered) corresponds to the emission from excitation at 30 000 cm^{-1} (singlet LMLCT). The metal-centered excitation at roughly 25 600 cm^{-1} corresponds to the triplet state in the monomer or the dimer **A** and subsequent emission from the dimer at 17 900 cm^{-1} (MLCT). Emission at 15 500 cm^{-1} (MLCT) accompanied by less intense emission from the above triplet excited states of dimer **A** would be produced if excitation at 23 000 cm^{-1} (MLCT) occurs. These MLCT states were centered mostly on the biphenyl ligand. The lowest energy emission reported (at ca. 13 500 cm^{-1}) was metal centered and can be assigned to a triplet excitation at 20 000 cm^{-1}. We suggest that the low-energy triplet excited state of the monomer (at 13 000 cm^{-1}) is not emissive and is associated with a $\pi \rightarrow \pi^*$ derived excited state, whereas all of the above processes were based on metal-centered excited states. All triplet excited states of dimer **A** were found to correspond to reported peaks in the emission spectrum of the complex except the lowest energy excited state which fell out of the range of reported data. Considering that the dimer peaks are all MLCT transitions and based on a numerical comparison of the peak positions, we can state that in concentrated solution the emitting species is the dimer.

The emission energies and the band broadness ($\Delta\omega_{1/2} =$ 970 cm^{-1}) in the simulated emission spectrum of dimer **A** (Figure 7) were found to be in a good agreement with the experimental ones. The TDDFT computational interpretation of the emission behavior was impressive.

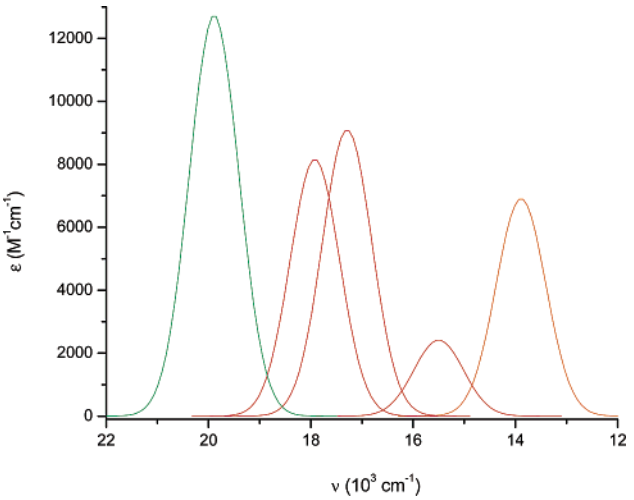

Figure 7. Simulated spectrum of dimer **A** of [Pt(bph)(CO)$_2$] based on Gaussian curves for five triplet excited states from Table 3B (based on the triplet ground state) in wavenumbers versus oscillator strength. Line colors: Pt → delocalized, orange; MLCT, red; Pt centered, olive.

On the basis of the above results, it can be concluded that the primary absorbing species in solutions of [Pt(bph)(CO)$_2$] are the monomer at lower concentration and dimer **A** at higher concentration. The emission in concentrated solution is due to the triplet dimer **A**. The high-energy excitations are due to triplet−triplet transitions in the monomer ($E >$ 25 000 cm^{-1}) at higher energy and in dimer **A** at lower energy ($E <$ 25 000 cm^{-1}).

Conclusion

DFT-calculated geometries of the monomer, dimer, and trimer of [Pt(bph)(CO)$_2$] were found to correlate relatively well with the geometry of the single crystal reported. The energies and the geometries of four possible dimers were evaluated, and it was confirmed that dimer **A** was the most stable one. Significant deviation from planarity was described, likely to accommodate the Pt−Pt binding. A 4.0% shortening of the metal−metal bond upon the transition from the singlet ground to the lowest-lying triplet state was reported. TDDFT was utilized for the purpose of interpreting the spectroscopic behavior of the complex in solution. On the basis of the excited-state energies and the oscillator strengths, singlet and triplet excited-state spectra were calculated using Gaussian curve-fitting methods for the monomer and dimer **A**. After a careful analysis it was concluded that the monomer would be the primary absorbing species at low concentration. In concentrated solution the dimer **A** would be the primary absorbing species and the triplet dimer **A** would be the emitting species.

Acknowledgment. We acknowledge the support of Kansas NSF Cooperative Agreement EPS-9874732, the Wichita State University High Performance Computing Center, the Wichita State University Office of Research Administration, the Department of Energy, and Parker Fellowships (S.R.S. and J.M.V.).

IC030084N